Lab on a Chip

Accepted Manuscript

ROYAL SOCIETY OF CHEMISTRY

www.rsc.org/loc

SAW-based fluid atomization device suitable for economic mass-scale production using a fluid supply via on-chip embedded SU-8 microchannels.

Lab on a Chip

RSCPublishing

ARTICLE

SAW-based fluid atomization using mass-producible chip devices

Cite this: DOI: 10.1039/x0xx00000x

A. Winkler, S. M. Harazim, S. B. Menzel, and H. Schmidt

Received 00th January 2012,
Accepted 00th January 2012

DOI: 10.1039/x0xx00000x

www.rsc.org/

Surface acoustic wave (SAW) based fluid atomizers are ideally suited to generate micrometer-sized droplets without any moving parts or nozzles. Versatile application fields can be found for instance in biomedical, aerosol or thin film technology, including medical inhalators or particle deposition for advanced surface treatment. Such atomizers also show a great potential for on-chip integration and can lead to an economic production of hand-held and even disposable devices, with either a single functionality or integrated in more complex superior systems. However, this potential was limited in the past by fluid supply mechanisms inadequate regarding mass-production, accuracy and reliability. In this work, we briefly discuss existing fluid supply methods and demonstrate a straightforward new approach suited for reliable and cost-effective mass-scale manufacturing of SAW atomizer chips. Our approach is based on a fluid supply at the boundary of the acoustic beam via SU-8 microchannels produced by a novel one-layer/double-exposure photolithography method. Using this technique, we demonstrate precise and stable fluid atomization with almost ideal aerosol plume geometry from a dynamically stabilized thin fluid film. Additionally, we demonstrate the possibility to *in-situ* alter the droplet size distribution by controlling the amount of fluid available in the active region of the chip.

Introduction

The concept of fluid atomization using surface acoustic waves was already demonstrated by Kurosawa et al in 1995[1,2]. Since then, this phenomenon has been investigated in various scientific publications, regarding the underlying physical phenomena[3-5] or possible applications, including inhalation therapy[6-8], olfactory displays[9-11], micro- and nanoparticle synthesis[12-18], thin film deposition[19,20] and mass spectroscopy of non-volatile fluids[21-24]. Despite the broad variety of attractive applications and previous work detailing the mechanisms of SAW atomization, still no commercial SAW-based fluid atomizer is available after 20 years of research. The reason for this could be attributed to economic and technological limitations regarding the miniaturization and mass-producibility of conventional fluid supply techniques and the radio-frequency (RF) signal source. While the issue of miniaturization of the RF signal source has meanwhile been solved using accurately designed and dedicated electronics as well as optimized interdigital transducers and signalling schemes[8,25,26], the fluid supply has not yet been either improved or miniaturized.

In principle, SAW-based fluid atomization is the result of the interaction of an acoustic wave on the surface of a piezoelectric substrate with a fluid placed in its propagation path, i.e. the acoustic beam. Various acoustofluidic effects can take place in such a setup, depending on the boundary conditions, including the SAW amplitude distribution and the geometrical shape and material properties of the fluid. Fine droplets with adjustable diameters between approximately 0.1 and 30 µm – a size range relevant for many applications – are acoustically ejected out of a thin fluid film, generated, stabilized and laterally extended by standing longitudinal pressure waves between the solid/fluid and the fluid/air interface[3]. This thin fluid film thereby can be regarded as a body of fluid with a height level in the order of the acoustic wavelength and substantially smaller than any of its horizontal dimensions. When a fluid body with increased dimension, i.e. a fluid "volume", is present in the region of high acoustic energy, i.e. the center of the SAW beam, additional acoustofluidic effects including jetting and Rayleigh streaming arise[27]. An ideal fluid supply would therefore limit the fluid geometry to a thin film in the central region of the acoustic beam, i.e. the aperture (in a first approximation). Additionally, it should provide for a reproducible and stable aerosol generation, together with a simple and cost-effective device production on the industrial scale. As SAWs have wavelengths below some hundred micrometers, also their wavefields exhibit features on this scale, including such caused by interference and diffraction or the pressure (anti-)nodes of standing SAW. As the SAW wavefield-fluid interaction is the origin of the aerosol formation, an extraordinary accuracy of the fluid supply position and geometry with respect to the local wavefield properties is essential to ensure the device operation reproducibility and predictable aerosol properties.

In order to realize a fluid supply to the chip surface in SAW-based fluid atomization, three different methods have been

mentioned in the literature until now: **(1)** In the first approach, individual droplets are delivered to the chip surface via capillaries or tubes[4,6,9,12-17,21,22,24,28-36]. This technique is very simple, but delivers the fluid in the form of a "volume" to the chip surface. If the fluid wetting is not controlled by structured thin films (e.g. Perfluorosilanes), the achieved drop position and the drop shape are not reproducible with respect to the local SAW wavefield. Additionally, because the droplet volume reduces during atomization, this method does not lead to a continuous aerosol production or constant aerosol properties.
(2) In the second approach, fluid wetted tissues or capillaries are placed directly on the chip surface[3,5,8,18,19,21,26,30,31,37]. The fluid then forms a meniscus around the tissue or capillary, which interacts with the SAW. This technique is relatively simple to implement and already leads to a continuous aerosol generation. Unfortunately, when the tissue is placed in the SAW beam, it does not deliver the fluid entirely in the desired form of a thin film and imposes additional acoustic boundary conditions. So far, the effect of the interaction of the SAW with the fibres of the tissue or the capillary material is unclear. However, the interaction cannot be neglected when high reproducibility and process control are required, especially when the fibre and pore diameters of the tissue, or the opening and wall thickness of the capillary, are in the order of the SAW wavelength. Additionally, fibres could impose a filter effect on dispersions or solutions. Although this technique has proven its suitability for use in experiments to elucidate the process of atomization or certain applications, the characterization, miniaturization and reproducible positioning of the tissue is as difficult to realize, as it is mandatory for a mass-scale production.

(3) A third – and rarely used – approach introduced by Kurosawa et al.[1,2] and Soluch et al.[25,38], is based on capillary slits of 10 to 50 µm height and several mm width, formed between the piezoelectric substrate and a glass cover slip. Compared to the approaches 1 and 2, the continuous fluid supply via capillary slits has one mentionable advantage: It supplies the fluid to the SAW beam in form of a thin film, i.e. the basis for the SAW fluid atomization process, whereby the fluid height at the slit outlet is adjustable via the capillary slit height. However, the original approaches also show several drawbacks, which may explain why the technique has not found widespread application. These drawbacks include a complicated and time-consuming manual fixation of glass cover slips on the chip surface (which in an industrial approach would be covered by a slow serial pick and place process), an inaccurate slit placement with respect to the local properties of the acoustic wavefield and low control over the precise slit dimensions.

Our new approach **(4)** is based on a fluid supply via on-chip polymeric microchannels prepared by photolithography directly on the chip surface. As the feature resolution and placement accuracy of photolithography can be on the sub-micrometer scale, this technique allows a highly reproducible channel placement with respect to the local acoustic wavefield properties. In addition to the control of the fluid height boundary condition with capillary slits, the use of microchannels also enables control over the lateral fluid dimensions in the acoustic path. To further improve the aerosol formation process, our approach makes use of the local wavefield properties with a fluid supply at the boundary of the acoustic beam, not demonstrated before. In contrast to the center of the acoustic beam (i.e. within the SAW aperture in a first approximation) with high local SAW displacement amplitudes, only small amplitudes exist at its boundary regions, so atomization will not occur here. However, due to the existing amplitude gradient, caused by SAW diffraction, directed towards the center of the beam, fluids positioned at the acoustic boundary are drawn into the beam center and atomized in a region with sufficiently high local SAW amplitude. Due to this, a spatial separation of the fluid supply zone at the boundary of the acoustic beam and the atomization zone in the beam center improves both, the aerosol generation process and the aerosol properties. Additionally, materials placed at the boundary of the acoustic beam, e.g. the walls of microfluidic channels, undergo less mechanical stress and less heating / degradation due to a much lower absorption of acoustic energy (data not shown here). The SU-8 channels prepared in this work are therefore placed in the boundary region of the acoustic beam, with channel outlets oriented in direction perpendicular to the SAW propagation direction.

The use of photolithographically patterned microchannels allows the parallel and cost-effective device manufacturing in a wafer-scale fashion using materials compatible to most relevant fluids and biological systems. Our photoactive polymer material of choice, the photostructurable expoxy SU-8 (Microchem Corp.), exhibits optical transparency, excellent chemical resistance, and high mechanical and thermal stability. Also, the biocompatibility of SU-8 was recently verified by several in-vitro and even in-vivo studies[39-43]. Due to these outstanding properties, SU-8 should be suited for most technical aerosol generation systems.

Experimental

A pair of opposing interdigital transducers (65 MHz, 1 mm aperture, 6 mm spacing) matched to 50 Ω impedance by design and consisting of subsequent layers of Ti (5 nm) and highly-textured Al (295 nm) was prepared on 128°YX-$LiNbO_3$ substrate (128° rotated Y-cut Lithium Niobate with X-propagation direction; 8x14 mm² size) via electron-beam evaporation and lift-off technique. A one µm thick SiO_2 layer was sputter-deposited onto the chip surface in order to prohibit corrosion of the IDT electrodes and to establish a surface with high biocompatibility on the piezoelectric substrate[44]. SU-8-50 photoresist (Microchem Corp.) was spin coated on the chip surface, forming an 80 µm thick layer, and subsequently prebaked at 95°C on a hot plate. Contact lithography was carried out in a two-step fashion: Using a first mask, the channel walls were defined at a wavelength of 320-365 nm with a dose of 7 mW/cm² for 20 s exposure time. At this wavelength, SU-8 is sufficiently transparent to enable an exposure of the whole film thickness. The low dosage was necessary to prohibit reflexions from the backside of the transparent $LiNbO_3$ substrate, otherwise creating unwanted features on the channel sidewalls. An intermediate temperature treatment (same conditions as prebake) was carried out to cross-link the exposed resist areas making the SU-8 structures optically visible due to different refractive indices of exposed and unexposed SU-8. Using a second mask aligned to the structures of step 1, the channel cover lid was defined at a wavelength of 254 nm with a dose of 2 mW/cm² for 10 s exposure time. At this wavelength, the SU-8 is almost opaque. Thus, only the uppermost region (few µm) of the polymer film is exposed and hardened. After the lithography, a soft bake at 95°C was carried out, the

structures were finally developed in mr-DEV 600 (micro resist technology GmbH, Germany) and the chips were cleaned in isopropyl alcohol and dried in air. This one-layer/double-exposure approach[45] is much faster and easier to carry out as compared to the conventional SU-8 lithography, requiring two individual steps each comprising resist deposition, pre-/soft-bake, exposure and development. The SU-8 structures (Fig. 1) were designed in a drop-like geometry, in order to enable a sufficient mechanical stability of the channel walls at the channel outlet and to minimize the effective polymer cross section in the acoustic beam at the same time – thereby minimizing the SAW-SU-8 interaction and associated energy uptake by the channel walls.

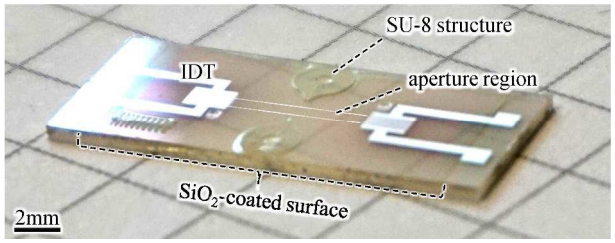

Fig. 1. SAW chip for fluid atomization with microchannels integrated in drop-like SU-8 polymer structures, located outside of the acoustic aperture, i.e. in the boundary region of the acoustic beam

The chip was mechanically fixed on a CNC milled and anodized aluminium platform using double-sided carbon tape (Tesa Germany) and electrically contacted using printed circuit board conductor plates with stripe lines matched to 50 Ω impedance and gold spring pins. High frequency signals were supplied via SMA cables from a dual-channel PowerSAW signal source (BelektroniG GmbH, Germany) at matched operation frequency of 64.3 MHz with a load power of 3 W supplied to each IDT. For the fluidic connection, two different approaches were used: (1) for first tests, slightly conic PMMA tubes (1 mm diameter, 5 mm length) were glued on top of the SU-8 using Vitralit 7041 resin (Panacol-Elosol GmbH) and subsequent UV curing. Silicon tubing was attached to the PMMA tubes (setup of Fig. 4). This setup is well suited for lab purposes, but a more straight-forward approach (2) was also successfully tested (setup shown in Fig. 2; also used for droplet size measurements).

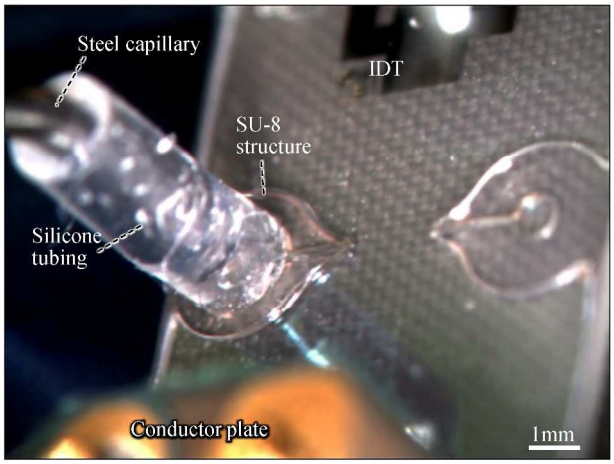

Fig. 2. Fluidic interconnection between microchannel and reservoir/pump via a silicone tube pressed directly onto the SU-8 structure

Here, a direct connection of the SU-8 structures to an external reservoir was realized by silicon tubing mounted on a steel tube and directly pressed on the SU-8 structures – equal to the interconnection via a sealing ring. While the SU-8 cover lid, i.e. the channel cover, has a thickness of only few micrometers, it shows sufficient mechanical stability to withstand any damage even after several cycles of connecting and disconnecting the silicone tubing. This approach allows for simple device preparation, fast chip exchange, better device integration and further reduction of the device manufacturing costs.

Characterization of the atomized fluid with respect to the aerosol droplet size distribution in the range of 1 to 100 µm was carried out using a Helos KR laser diffractometer (Sympatec GmbH, Germany). The aerosol beam was measured for 90 s in a distance of 25 mm to the chip surface with a laser spot of approximately 20 mm diameter. A suction device was used to collect the aerosol above the measurement spot in order to prohibit fluid condensation on the diffractometer lenses. Droplet sizes were calculated using the Mie scattering theory. The dependence of the droplet size distribution on the fluid flow rate (50 to 400 µl/min) was investigated using deionized water as a model fluid delivered by a neMESYS syringe pump (Cetoni GmbH, Germany). Additionally, an application-relevant inhalation solution (Emser solution, Heilwasser und Quellenprodukte des Staatsbades Bad Ems GmbH & Co. KG, Germany), containing 1.175 g of salts per 100 ml cleaned water was atomized at a flow rate of 100 µl/min and characterized regarding the achieved droplet size distribution.

Results & discussion

The produced microchannels show an accurate rectangular cross-section with SU-8 walls and cover lid, and SiO_2 bottom (see Fig. 3). The outer lateral dimensions of the SU-8 structures were 2.5 mm x 3 mm, while the embedded microchannel had lateral dimension of 100 µm x 1.4 mm. The microchannel side facing to the chip center is open and positioned at a distance of 675 µm from the chip center, i.e. 175 µm from the aperture edge. The opposite side of the microchannel ends in a circular reservoir of 700 µm diameter with no cover lid. The SU-8 lid covering the channel was found to have a thickness of only about 5 µm and a convex shape, due to compressive stress in the SU-8 layer after curing. However, due to the excellent mechanical stability of SU-8, the thin cover lid is not damaged even at fluid flow rates of up to 400 µl/min. As the microchannel walls have a width of 40 µm at their outlet, representing only two-thirds of the SAW wavelength, the interaction with the SAW and the accompanied energy absorption leading to polymer heating, wave damping and polymer degradation is minimized. A further reduction of the SU-8 wall thickness should be possible.

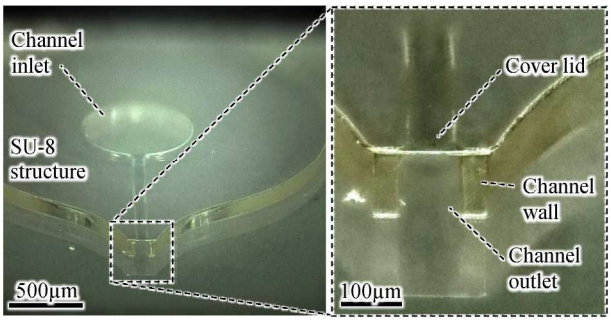

Fig. 3. SU-8 polymer structure with embedded microchannel: complete structure and magnification of channel outlet

The observed aerosol formation process using a boundary fluid supply can be described as follows: When a fluid is supplied to the microchannel on the smooth chip surface, if forms a meniscus at the channel outlet with the width and height of the channel and a contact angle defined by Young's equation[46]. On application of the sinusoidal signal to the IDTs, two opposing SAWs of the Rayleigh type are excited on the chip surface, forming a standing surface acoustic wave (sSAW) field around the channel outlet. The fluid meniscus at the boundary of the acoustic beam thereby experiences a positive displacement amplitude gradient directed towards the amplitude maximum in the center of the acoustic beam. This gradient is caused by the SAW diffraction. Due to a standing longitudinal wave formed between the solid-liquid and the liquid-air interfaces, a thin fluid film with a height in the order of the acoustic wavelength in the fluid is dynamically generated and stabilized[3]. The amplitude gradient leads to its lateral spreading into the beam center, where atomization takes place due to the sufficiently high displacement amplitude by destabilization of the fluid film surface. As only the thin fluid film is present in the acoustic beam, secondary effects like streaming, fluid accumulation or jetting are diminished and the aerosol generation takes place under favourable conditions.

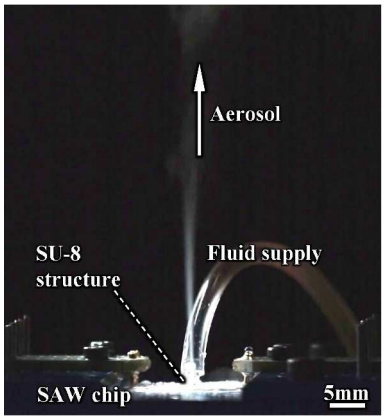

Fig. 4. sSAW-based fluid atomization using on-chip SU-8 microchannels: side view on experimental setup showing a vertical 50 mm high aerosol plume with an opening angle of approximately 5°

Fig. 4 shows the resulting aerosol plume formed with an almost ideal shape regarding the low opening angle of only about 5° and a height of approximately 50 mm (see also supplementary videos 1 and 3). The aerosol was produced here with an application-relevant rate of about 100 µl/min. Fig. 5 shows a magnified detail of the laterally separated zones of fluid supply and atomization, acquired by an optical stereomicroscope inclined under 45° angle with respect to the surface normal (see also supplementary video 4). One can clearly identify the channel outlet at the boundary of the acoustic beam (region 2), the atomization zone in the center of the acoustic beam (region 1) and the interconnecting, dynamically stabilized fluid thin film. The lateral extension and the height of this thin film on the surface is limited by the local SAW amplitude and the fluid flow rate. The thin film height was not directly measured, but estimated from microscopic images to be below 10 µm, a value comparable to earlier predictions for thin film formation at the used SAW wavelength[3].

Due to atomization of the thin fluid film, the amount of fluid is drastically reduced in region 1. Therefore, the fluid increasingly resembles the standing SAW wavefield pattern with increasing distance to the channel outlet until no fluid is left on the chip surface. As the interconnecting thin film dimensions are stabilized by the SAW, fluid is pulled out of the microchannel during the atomization process. This self-containing fluid supply mechanism was already described in other publications and makes the use of an external pump obsolete, provided the pressure drop along the tubing does not limit the fluid outflow and the fluid pressure at the channel outlet is low enough to prevent flooding of the chip surface. However, the use of an external pump can improve the aerosol formation process, as will be described in the following.

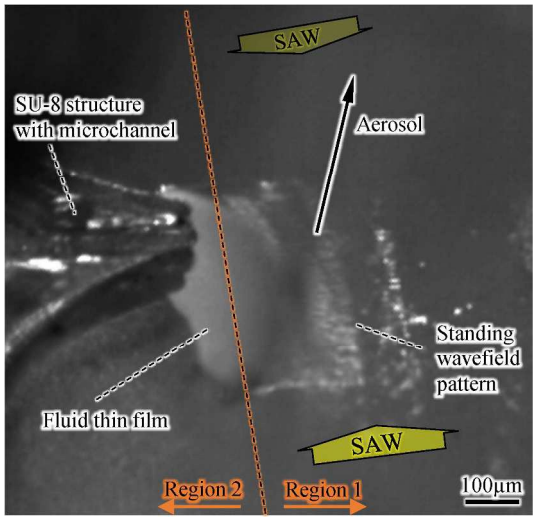

Fig. 5. Tilted microscopic image showing the steady state of sSAW-based fluid atomization with an SU-8 microchannel fluid supply: Magnification of channel outlet (in region 2), atomization zone (in region 1), the interconnecting fluid thin film, the aerosol mist and the standing wavefield pattern, resembled by the fluid in region 1

In Fig. 6, the measured droplet size distribution is shown for varying flow rate, while all other parameters were kept constant. In general, the diffractometric data shows three existing peaks in the aerosol: a first peak below 3 µm containing 20 to 30% of the overall droplet volume, a second one – the main peak – between 3 and 50 µm containing 50 to 75% of the overall droplet volume and a third peak between 30 and 100 µm only existing for small flow rates.

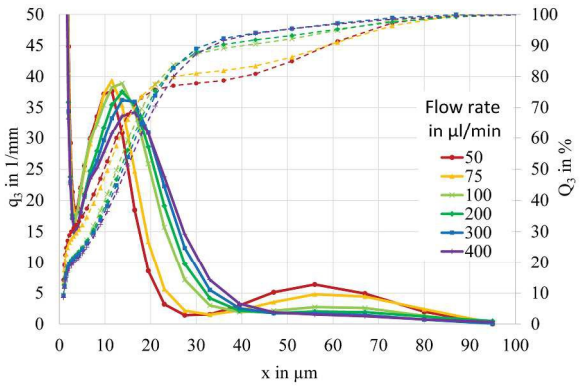

Fig. 6. Droplet size distributions (measured by laser diffractometry for different fluid flow rates through an SU-8 microchannel

Regarding the main peak, a gradual increase in the median droplet size from 10 to 15.5 µm can be seen when the flow rate is increased from 50 to 400 µl/min. The associated relative standard deviation increases only slightly from 80 to 90% in this range of the flow rate. The dependency of the droplet size from the flow rate was not shown in other publications, as conventionally the flow rate is only measured, but not directly controlled – or limited – as in the experiments shown here. The reason for the dependency of droplet size from the flow rate is assumed to be the change of the acoustically stabilized fluid thin film thickness: Collins et al. showed a dependency of the film thickness on the contact angle and the local wavefield properties, due to a balance between local radiation pressure intensity and capillary stress[3]. In turn, the thickness of the fluid film determines the droplet size in the aerosol. As the fluid flow rate limits the available amount of fluid on the chip surface, it influences the film dimension and, thus, the droplet size distribution obtained. Here, this limitation leads to a 50% increase of the median droplet size. It should be noted, that different possibilities of droplet size control were reported already or are probable to exist. These include the fluid parameters (e.g. density, viscosity, surface tension), the SAW wavelength / frequency, the IDT aperture, the IDT orientation, the addition of coatings, the chip surface chemistry and the type and properties of the fluid supply (e.g. channel dimensions, paper porosity, etc.). However, for an existing device and a specific fluid to be atomized, none of these parameters can be changed *in-situ*, i.e. during the device operation. For a given setup, the flow rate thereby represents another possible parameter for the *in-situ* droplet size control beside the SAW power (and if applicable the temperature) and thus, has a significant relevance for the development of future devices.

The origin of the fraction with the smallest droplets (first peak in Fig. 6) is not clear so far, but we assume them to be caused by droplet breakup, i.e. the splitting of larger droplets or jets into smaller ones, due to the exceeding of a critical Weber number of the droplets or jets moving through the ambient gas phase. Interestingly, the volume fraction of the smallest droplets gradually increases from 5 to 12% when the flow rate is reduced from 400 to 50 µl/s. The assumed change of the thin film geometry with the fluid flow rate also explains this effect: At constant SAW power, a reduced film height at reduced fluid flow will increase the spatial power density, which could lead to a higher velocity of the expelled droplets. This in turn increases their Weber number and the chance of their breakup into smaller droplets. While the large droplets of the third peak were not observed visually and their existence at a lower availability of fluid on the chip surface is unlikely, we cannot negate their existence at this stage of research. Their origin could be either a secondary droplet generation effect (e.g. fluid jetting), merging of smaller droplets or a measurement artefact, i.e. caused by the increase of the intermediate index of refraction in the aerosol at small droplet size distributions.

The atomization of the inhalation solution produced similar results: the first peak (< 3.5 µm droplet size) contained approx. 20% of the overall fluid volume, while the main peak (9.7 ± 8.1 µm droplet size) contained 68% of the overall fluid volume. Also, a peak with additional droplets with larger diameter (peak 3) was observed.

During the laser diffraction analysis, a device was operated for 20 min with water at varying flow rate and 5 min with the inhalation solution. After this time, the device was still operating and the SU-8 channels showed no significant degradation. Clogging of the active channel was not observed.

Conclusions

In SAW-based fluid atomization, the fluid supply method is of crucial importance for the aerosol formation process and the aerosol properties. In order to exploit the full potential of SAW fluid atomization technique for future devices, the incorporated fluid supply should deliver the fluid in the form of a thin film into the acoustic beam with extraordinary accuracy regarding its position and geometry with respect to the local wavefield properties. Additionally, it should provide a reproducible and stable device operation and a simple and cost-effective production. However, existing fluid supply methods are limiting the ability to produce devices at low costs on an industrial scale with high accuracy and reproducibility.

In order to enable the mass-scale manufacturing of SAW fluid atomizer devices, we demonstrated a promising fluid supply approach based on microchannels embedded in SU-8 structures, directly integrated on the chip surface. Utilizing the wavelength-dependent optical properties of unexposed SU-8, we established a novel photolithographic one-layer/double-exposure procedure for SU-8 on $LiNbO_3$ substrates, incorporating two separate light wavelengths and highly reduced exposure time. This technique is suitable for a wafer-scale production of SU-8 structures on transparent piezoelectric $LiNbO_3$ and not limited to SAW fluid atomization devices only. It ensures a maximum precision and reproducibility with respect to structure position and geometry. The produced SU-8 microchannels covered by a thin but mechanically very stable SU-8 lid are thereby perfectly suited for miniaturization. Furthermore, the SU-8 structures are compatible to higher-level microfluidic elements, e.g. external pumps or valves, using the easily realizable sealing ring interconnection demonstrated here.

A continuous fluid supply to the chip surface via photolithographically patterned microchannels allows maximum control over the dimensions (height and width) of the formed fluid meniscus and its exact position with respect to the local acoustic wavefield, i.e. the driving force for atomization, with a resolution in the sub-micrometer regime. The placement of the microchannels at the boundary of the acoustic beam minimizes the interaction of the channel wall material with the SAW and reduces SAW damping in the polymer material and therefore heating and stress-induced damage, which would inevitably occur when the polymer is placed in the center SAW beam. Due to the stabilization and extension of the thin fluid film out of the fluid meniscus by the SAW itself, a lateral separation of fluid supply and atomization zone can be achieved and was demonstrated here for the first time. Thereby, the aerosol droplets are produced directly out of the thin fluid film, which can be seen as an ideal atomization setup. The droplet size distribution can be optimized and the reproducibility of experiments is increased, as the fluid supply is no longer interacting with the high amplitude SAW.

Using our new fluid supply approach, we atomized water and an inhalation solution to fine droplets in an almost ideally shaped aerosol plume with low opening angle of only about 5°

and vertically aligned with respect to the chip surface due to the standing SAW wavefield applied. Measurements of the achieved droplet size distribution show a strong dependency of the droplet size on the fluid flow rate, reported here for the first time. Our results indicate that the flow rate is a highly interesting parameter for future devices requiring an *in-situ* droplet size control.

In summary, the fluid supply technique via SU-8 microchannels located at the boundary of the acoustic beam as well as the strategies for an optimized experimental setup described in this work complete a very promising approach for the economic mass-scale production of SAW fluid atomizer chips for hand-held and even disposable devices. After 20 years of research, SAW atomization devices for therapeutic and industrial applications with the ability to produce tailored aerosols finally is able to leave the lab scale.

Acknowledgements

This work was funded by the German Research Foundation (DFG Grant WI 4140/2-1) and the Federal Ministry of Education and Research (BMBF InnoProfile-Transfer 03IPT610A). The authors wish to thank L. Hillemann and A. Kupka from the research group "Mechanical Process Engineering" of the Dresden University of Technology for their assistance with aerosol measurements and helpful discussion.

Notes and references

IFW Dresden, SAWLab Saxony, PF 270116, 01171 Dresden, Germany,
Email: A.Winkler@ifw-dresden.de

Electronic Supplementary Information (ESI) available: Video 1 - "SAW-based water atomization using an on-chip SU-8 microchannel" in side view; Video 2: "SAW-based water atomization during laser diffraction measurement; top view"; Video 3: "SAW-based water atomization during laser diffraction measurement; side view"; Video 4 - "SAW-based water atomization: Magnification of the channel outlet and the atomization zone". See DOI: 10.1039/b000000x/

1 M. Kurosawa, T. Watanabe, A. Futami and T. Higuchi, *Sensors and Actuators A: Physical*, 1995, **50**, 69-74.
2 M. Kurosawa, T. Watanabe and T. Higuchi, in *Micro Electro Mechanical Systems - IEEE Proceedings*, 1995, pp. 25-30.
3 D. J. Collins, O. Manor, A. Winkler, H. Schmidt, J. R. Friend and L. Y. Yeo, *Physical Review E*, 2012, **86**, 1-9.
4 A. Qi, L. Y. Yeo and J. R. Friend, *Physics of Fluids*, 2008, **20**, 1-14.
5 D. Taller, D. B. Go and H. C. Chang, *Physical Review E*, 2013, **87**.
6 A. S. Qi, J. R. Friend, L. Y. Yeo, D. A. V. Morton, M. P. McIntosh and L. Spiccia, *Lab on a Chip*, 2009, **9**, 2184-2193.
7 L. Y. Yeo, J. R. Friend, M. P. McIntosh, E. N. T. Meeusen and D. A. V. Morton, *Expert Opinion on Drug Delivery*, 2010, **7**, 663-679.
8 A. Rajapaksa, A. S. Qi, L. Y. Yeo, R. Coppel and J. R. Friend, *Lab on a Chip*, 2014, **14**, 1858-1865.
9 Y. Ariyakul and T. Nakamoto, in *IEEE Virtual Reality Conference*, eds. M. Hirose, B. Lok, A. Majumder and D. Schmalstieg, IEEE, New York, 2011, pp. 193-194.
10 Y. Ariyakul and T. Nakamoto, *IEEE Sens. J.*, 2013, **13**, 4918-4923.
11 T. Nakamoto, K. Hashimoto, T. Aizawa and Y. Ariyakul, 2014.
12 M. Alvarez, J. R. Friend and L. Y. Yeo, *Nanotechnology*, 2008, **19**.
13 M. Alvarez, L. Y. Yeo, J. R. Friend and M. Jamriska, *Biomicrofluidics*, 2009, **3**, 1-12.
14 S. Anand, J. Nylk, C. Dodds, J. M. Cooper, S. N. Neale and D. McGloin, in *Optical Trapping and Optical Micromanipulation Viii*, eds. K. Dholakia and G. C. Spalding, Spie-Int Soc Optical Engineering, Bellingham, 2011, vol. 8097.
15 J. Ju, Y. Yamagata, H. Ohmori and T. Higuchi, *Sens. Actuator A-Phys.*, 2008, **147**, 570-575.
16 J. W. Kim, Y. Yamagata, M. Takasaki, B. H. Lee, H. Ohmori and T. Higuchi, *Sensors and Actuators B-Chemical*, 2005, **107**, 535-545.
17 K. C. Ng, A. S. Qi, L. Y. Yeo, J. Friend and W. L. Cheng, in *Smart Nano-Micro Materials and Devices*, eds. S. Juodkazis and M. Gu, Spie-Int Soc Optical Engineering, Bellingham, 2011, vol. 8204.
18 A. S. Qi, P. Chan, J. Ho, A. Rajapaksa, J. Friend and L. Y. Yeo, *ACS Nano*, 2011, **5**, 9583-9591.
19 N. Murochi, M. Sugimoto, Y. Matsui and J. Kondoh, *Japanese Journal of Applied Physics Part 1-Regular Papers Brief Communications & Review Papers*, 2007, **46**, 4754-4759.
20 M. Darmawan, K. Jeon, J. M. Ju, Y. Yamagata and D. Byun, *Sensors and Actuators A: Physical*, 2014, **205**, 177-185.
21 L. Bllaci, S. Kjellstrom, L. Eliasson, J. R. Friend, L. Y. Yeo and S. Nilsson, *Anal Chem*, 2013, **85**, 2623-2629.
22 S. R. Heron, R. Wilson, S. A. Shaffer, D. R. Goodlett and J. M. Cooper, *Anal Chem*, 2010, **82**, 3985-3989.
23 J. Ho, M. K. Tan, D. B. Go, L. Y. Yeo, J. R. Friend and H. C. Chang, *Anal Chem*, 2011, **83**, 3260-3266.
24 Y. Huang, S. H. Yoon, S. R. Heron, C. D. Masselon, J. S. Edgar, F. Turecek and D. R. Goodlett, *Journal of the American Society for Mass Spectrometry*, 2012, **23**, 1062-1070.
25 W. Soluch and T. Wrobel, *Electronics Letters*, 2006, **42**, 1432-1433.
26 A. Qi, L. Yeo, J. Friend and J. Ho, *Lab on a Chip*, 2010, **10**, 470-476.
27 L. Y. Yeo and J. R. Friend, *Annual Review of Fluid Mechanics, Vol 46*, 2014, **46**, 379-406.
28 M. Alvarez, J. R. Friend and L. Y. Yeo, *Langmuir*, 2008, **24**, 10629-10632.
29 J. Bennes, S. Alzuaga, S. Ballandras, F. Cherioux, F. Bastien and J. F. Manceau, in *IEEE Ultrasonics Symposium, Vols 1-4*, 2005, pp. 823-826.
30 K. Chono, N. Shimizu, Y. Matsui, J. Kondoh and S. Shiokawa, in *IEEE Ultrasonics Symposium Proceedings, Vol. 1 and 2*, eds. D. E. Yuhas and S. C. Schneider, 2003, pp. 1786-1789.
31 K. Chono, N. Shimizu, Y. Matsui, J. Kondoh and S. Shiokawa, *Japanese Journal of Applied Physics Part 1-Regular Papers Short Notes & Review Papers*, 2004, **43**, 2987-2991.
32 J. Y. Ju, Y. Yamagata, H. Ohmori and T. Higuchi, *Sens. Actuator A-Phys.*, 2008, **145**, 437-441.
33 M. Kurosawa, A. Futami and T. Higuchi, *Proceedings of Transducers Conference*, 1997, 801-804.
34 Y. Q. Fu, Y. Li, C. Zhao, F. Placido and A. J. Walton, *Applied Physics Letters*, 2012, **101**.
35 A. Qi, J. R. Friend and L. Y. Yeo, in *IEEE Ultrasonics Symposium International*, 2009, DOI: 10.1109/ultsym.2009.5441556, pp. 787-790.
36 Y. Zha and A. L. Zhang, in *2011 Symposium on Piezoelectricity, Acoustic Waves and Device Applications*, eds. H. Zheng, Y. Hu, C. Gao, W. Chen and T. Han, IEEE, New York, 2011, pp. 142-145.
37 T. Vuong, A. Qi, M. Muradoglu, B. H. P. Cheong, O. W. Liew, C. X. Ang, J. Fu, L. Yeo, J. Friend and T. W. Ng, *Soft Matter*, 2013, **9**, 3631-3639.
38 W. Soluch and T. Wrobel, *Electronics Letters*, 2003, **39**, 582-583.
39 S. H. Cho, H. M. Lu, L. Cauller, M. I. Romero-Ortega, J. B. Lee and G. A. Hughes, *IEEE Sens. J.*, 2008, **8**, 1830-1836.
40 M. Hennemeyer, F. Walther, S. Kerstan, K. Schurzinger, A. M. Gigler and R. W. Stark, *Microelectron. Eng.*, 2008, **85**, 1298-1301.
41 S. H. Huang, S. P. Lin and J. J. J. Chen, *Sens. Actuator A-Phys.*, 2014, **216**, 257-265.

42 K. V. Nemani, K. L. Moodie, J. B. Brennick, A. Su and B. Gimi, *Mater. Sci. Eng. C-Mater. Biol. Appl.*, 2013, **33**, 4453-4459.
43 M. Tijero, G. Gabriel, J. Caro, A. Altuna, R. Hernandez, R. Villa, J. Berganzo, F. J. Blanco, R. Salido and L. J. Fernandez, *Biosens. Bioelectron.*, 2009, **24**, 2410-2416.
44 A. Winkler, S. B. Menzel and H. Schmidt, *Proceedings of the SPIE: Smart Sensors, Actuators and MEMS IV*, 2009, 73621Q-73610.
45 J. M. Dykes, D. K. Poon, J. Wang, D. Sameoto, J. T. K. Tsui, C. Choo, G. H. Chapman, A. M. Parameswaren and B. L. Gray, 2007, vol. 6465, pp. 64650N-64650N-64612.
46 T. Young, *Philosophical Transactions of the Royal Society of London*, 1805, **95**, 65-87.